Nanoscale Advances

ROYAL SOCIETY OF CHEMISTRY

PAPER

View Article Online
View Journal | View Issue

Cite this: *Nanoscale Adv.*, 2024, **6**, 5042

Assessment of the drug delivery potential of graphene, boron nitride and their in-plane doped structures for hydroxyurea anti-cancer drug *via* DFT study

Mehedi Hasan Opi, Tanvir Ahmed, Mithila Roy Swarna, Afiya Akter Piya and Siraj Ud Daula Shamim *

Globally, cancer is the most common cause of mortality among all deadly diseases. As a result, a nanotechnology-based drug delivery system is used to improve the efficacy of cancer treatment, which provides an improved therapeutic index and delivers multiple drugs directly to the tumor site. In the present work, DFT calculations were employed to investigate the surface adsorption of a hydroxyurea (HU) anticancer drug on pristine graphene (GP), boron nitride ($B_{24}N_{24}$), and doped GP by replacing some of its carbon atoms with boron (B) and nitrogen (N) atoms to form $C_{30}B_9N_9$, $C_{16}B_{16}N_{16}$, and $C_6B_{21}N_{21}$ nanosheets. In gas media, HU is adsorbed on these $C_{30}B_9N_9$, $C_{16}B_{16}N_{16}$, $C_6B_{21}N_{21}$, and $B_{24}N_{24}$ nanosheets with adsorption energies of −0.70, −3.03, −2.47, and −1.96 eV, respectively. Alternatively, in water solvent media, the adsorption energies of $C_{30}B_9N_9$, $C_{16}B_{16}N_{16}$, $C_6B_{21}N_{21}$, and $B_{24}N_{24}$ are −0.82, −0.29, −0.15, and −0.26 eV, respectively. The energy gaps of the nanosheets were found to be 0.288, 0.174, 0.14, and 4.562 eV before adsorption, respectively. After the adsorption of HU on the proposed nanosheets, the energy gap was reduced to 0.15 eV for $C_{16}B_{16}N_{16}$. According to the DOS spectra, noticeable peaks appeared in the Fermi level after the adsorption of HU on the nanosheets, which indicates the reduction of the energy gap. Quantum molecular analysis predicted that the chemical potential, electrophilicity index, and nucleophilicity index of $C_{16}B_{16}N_{16}$ increased, whereas global hardness decreased, indicating high reactivity. Therefore, it can be concluded that among the proposed nanosheets, $C_{16}B_{16}N_{16}$ would be an appropriate carrier for the HU drug.

Received 22nd May 2024
Accepted 30th July 2024

DOI: 10.1039/d4na00428k

rsc.li/nanoscale-advances

1. Introduction

Cancer is currently the number one cause of death worldwide among all deadly diseases. With the world population growing rapidly, the number of new cancer cases has been increasing over the years. According to a study conducted in 2022, an estimated 20 million new cases and 9.7 million cancer-related deaths occur annually.[1] The development of cancer involves the loss of control over the cell cycle, which occurs when cell proliferation becomes uncontrollable and invading cells start spreading to other parts of the body.[2] The most common treatments for cancer include chemotherapy, radiotherapy, and surgery.[3] Chemotherapy is a treatment that aims to destroy cancerous cells. However, it can also harm normal cells, leading to side effects such as fatigue, hair loss, nausea, and vomiting.[4–6] Various chemotherapeutic drugs that are used for cancer treatment are called anticancer drugs.[7] Hydroxyurea (HU) is an orally administered anti-cancer drug that is effective and has a short-term toxicity profile in most patients.[8] Dresler and Stein synthesized HU for the first time in 1869.[9] It was later used as an anti-tumor agent in the 1960s[10] and is currently used to treat various conditions, such as leukemia,[11] sickle cell anemia,[12] HIV infection,[13] essential thrombocythemia,[14] psoriasis,[15] and polycythemia vera.[16] However, due to its lack of selectivity, it may cause adverse effects such as gastrointestinal disturbance, bone marrow suppression, and dermatological reactions.[10]

To minimize these adverse effects and improve the effectiveness of drugs, researchers are exploring the use of nanomaterials as drug carriers. Different nanomaterials, including zero-dimensional (0D), one-dimensional (1D), and two-dimensional (2D) materials[17] are being tested for drug delivery. Among these, 2D nanomaterials are particularly promising because of their large surface area, carrier mobility, solubility, and exceptional electrical and thermal conductivity.[18] Graphene-based 2D nanomaterials, in particular, have attracted much attention owing to their unique properties and wide range of applications.[19,20] Guo *et al.* synthesized graphene nanosheets using exfoliated graphite oxide as a precursor in

Department of Physics, Mawlana Bhashani Science and Technology University, Tangail, Bangladesh. E-mail: sdshamim@mbstu.ac.bd

their experiments.[21] Graphene nanosheets are a promising material for various applications, such as sensors, emitters, nanoelectronics, nanocomposites, and drug delivery.[22,23] However, there are some challenges to using it for drug delivery, primarily due to its poor dispersibility in water.[24] Additionally, the intrinsic toxicity of graphene is a serious concern that needs thorough investigation before its use in biomedical applications.[25–27] The surface chemistry of nanomaterials plays a crucial role in the biocompatibility and regulated behavior of drugs. Therefore, modifications in graphene are necessary to overcome these problems.[28] It has been reported that graphene nanosheets have low interaction with various substances.[29] Hence, the doping process is one of the most effective ways to enhance the reactivity of graphene nanosheets.[30]

In previous research, scientists improved graphene nanosheets by adding boron (B) and nitrogen (N) atoms to create heterostructures,[31] and it was found that the addition of heteroatoms improved the interaction behavior of the nanosheets.[32] Recently, in 2023, Ramasamy *et al.* researched the effect of defects and Si-doping on graphene sheets.[33] They claimed that defective and Si-doped graphene is more suitable than pristine sheets as a carrier for drug delivery. Louis *et al.*[34] also investigated the use of heteroatom (B, N, S)-doped graphene quantum dots as a possible drug carrier for isoniazid using Density Functional Theory (DFT). They observed substantial interaction between the doped graphene and the drug. On the other hand, hexagonal boron nitride nanosheets (BNNS), often referred to as "white graphene", have an analogous structure to graphene, featuring a honeycomb lattice where boron (B) and nitrogen (N) atoms replace carbon (C) atoms in sp^2-bonded two-dimensional (2D) layers.[35,36] BNNS possess several critical advantages over graphene, including a wide band gap, large surface areas, high thermal conductivity, excellent mechanical strength, high structural and chemical stability, high oxidation resistance, good chemical inertness, and lower toxicity.[37–40] These unique properties have garnered significant attention, leading to their use in various fields, such as dielectric materials,[41] catalysts,[42] composite materials,[43] electrochemical sensors,[44] and hydrogen storage elements.[45] Additionally, recent experimental studies have highlighted BNNS as a promising drug delivery system.[46–48] Their high biocompatibility and impressive performance in loading, releasing, and delivering anticancer drugs suggest promising applications in biological and biomedical fields. Consequently, BNNS are being extensively researched as potential drug carriers targeting cancer cells, paving the way for developing a new generation of drug delivery systems.

In our present work, we have investigated the surface adsorption of the HU anticancer drug on the pristine graphene (GP), boron nitride ($B_{24}N_{24}$) nanosheet, and doped GP by replacing some of its carbon atoms with boron (B) and nitrogen (N) atoms, at doping concentrations of 37.5%, 66.67%, and 87.5%, respectively, to form $C_{30}B_9N_9$, $C_{16}B_{16}N_{16}$, and $C_6B_{21}N_{21}$ nanosheets. The aim of this study was to increase the selectivity and reactivity of these nanosheets towards HU. In this simulation, we investigated the drug-loading mechanism, along with the electronic and structural properties of the nanosheets and complexes. Our aim was to find the most suitable carrier for HU by studying the adsorption energy, charge transfer, energy gap, electron density (ED) and electrostatic potential (ESP) maps. In order to gain a deeper understanding of the energy gap, we examined the density of states (DOS) and partial density of states (PDOS) spectra. Quantum molecular descriptors, such as the chemical potential (μ), global hardness (η), global softness (s), and electrophilicity index (ω), have been analyzed to predict the reactivity of the nanosheets toward HU. We also analyzed the effects of the solvent using the Conductor-like Screening Model (COSMO).

2. Computational details

All calculations in the present study were performed using the spin-unrestricted DFT framework in the DMol3 module in both air and water media.[49,50] Generalized gradient approximation (GGA) was chosen instead of local density approximation (LDA) in order to optimize the structures of the nanosheet, along with the complexes of HU,[51] because it has been shown in several prior research studies that LDA inflates findings for the equilibrium distance and bond energy.[52] DFT calculations are crucial for comprehending the electronic structure and properties of molecules.[53] DFT provides a quantum mechanical method used to investigate the electronic distribution within atoms and molecules, which in turn determines their chemical reactivity, stability, and physical characteristics. One of the key inputs required for DFT calculations is a model for the exchange–correlation interaction between electrons. The Perdew–Burke–Ernzerhof (PBE) functional is a widely used model that accounts for both the exchange and correlation effects within the GGA framework.[54] For better accuracy than the 6-31G(d,p) basis set in Gaussian, the DFT semi-core pseudopotential with a double-numerical basis set with polarization (DNP) was utilized in the core treatment.[55,56] The DNP basis set can minimize or even eliminate the basis set superposition error (BSSE).[57] To study the solvent effect of the nanosheets and complexes, water medium was used with a dielectric constant of 78.54.[58] The solvent effect was predicted using the COSMO technique.[59]

Adsorption is defined as a surface phenomenon in which the adsorbate species from the solution accumulate on the solid adsorbent surface by van der Waals interaction, and it is mainly a consequence of the surface energy. The energy (E_{ad}) of HU to get adsorbed on the surface of C_{48}, $C_{30}B_9N_9$, $C_{16}B_{16}N_{16}$, $C_6B_{21}N_{21}$ and $B_{24}N_{24}$ nanosheets is defined as follows:[60]

$$E_{ad} = E_{com} - E_{drug} - E_{nanosheet} \quad (1)$$

In the above equation, the symbols E_{com}, E_{drug} and $E_{nanosheet}$ denote the total energies of the complexes, HU drug, and nanosheet, respectively. The electronic properties are well defined by the energies of the lowest unoccupied molecular orbital (LUMO) and the highest occupied molecular orbital (HOMO), denoted by E_L and E_H, respectively. The energy gap fluctuations and the relation among these parameters are described as follows:

$$E_g = E_L - E_H \quad (2)$$

The quantum molecular descriptors, such as global hardness (η),[61] global softness (s),[62] chemical potential (μ),[63] electrophilicity index (ω),[64] and nucleophilicity index (υ)[65] were also calculated to predict the reactivity of the nanosheets toward HU by the following equations:

$$\text{Hardness, } \eta = (E_{LUMO} - E_{HUMO})/2 \quad (3)$$

$$\text{Softness, } s = 1/2\eta \quad (4)$$

$$\text{Chemical potential, } \mu = -(E_{LUMO} + E_{HOMO})/2 \quad (5)$$

$$\text{Electrophilicity index, } \omega = \mu^2/2\eta \quad (6)$$

$$\text{Nucleophilicity index, } \upsilon = 1/\omega \quad (7)$$

An investigation was carried out to determine if the structures after adsorption were in real local minima. This was done by analyzing the normal mode of vibrations. The study also involved analyzing the charge transfer between the drug and nanosheets using Hershfield charge analysis. This helped to determine if HU acted as a donor or acceptor. The interaction between HU and the nanosheets in a water solvent was studied using a dielectric constant of 78.54 and COSMO.

3. Results and discussion

3.1. Optimized geometric structures

To investigate the two-dimensional in-plane heterostructures, isolated pristine graphene (with 16 hexagons and 48 carbon atoms) and the boron nitride ($B_{24}N_{24}$) nanosheet have been chosen as our model structure. Then, the pristine graphene nanosheet has been modified with alternative B and N with doping concentrations of 37.5%, 66.67%, and 87.5%, respectively, to form $C_{30}B_9N_9$, $C_{16}B_{16}N_{16}$, and $C_6B_{21}N_{21}$ nanosheets. A comparative analysis was carried out among the five model nanosheets, involving one pristine graphene (C_{48}) and their three heterostructures ($C_{30}B_9N_9$, $C_{16}B_{16}N_{16}$, $C_6B_{21}N_{21}$) and the $B_{24}N_{24}$ nanosheet. The optimized geometries of these nanosheets are shown in Fig. 1.

The average bond length of C–C in GP was 1.413 Å, which was consistent with a previous study.[65] The bond length of C–H was 1.093 Å and was in good agreement with a prior study.[66] In addition, the bond angles of C–C–C and C–C–H in graphene were 120.09° and 118.85°. When GP was doped with alternative B and N, the average bond lengths of B–N, C–B and C–N are 1.409 Å, 1.51 Å and 1.372 Å, respectively. The bond angle of C–B–N is 120.36°.

The HU drug molecule contains two oxygen and two nitrogen atoms, which are numbered O1, O2, N1 and N2, respectively. The optimized geometry of the HU drug is also shown in Fig. 1(f), in which the bond lengths of N1–C, N2–C, and N2–O2 are found to be 1.380 Å, 1.40 Å, and 1.425 Å, respectively, and the bond angles of N1–C–O1 and N1–C–N2 are found to be 124.602° and 114.561°, respectively.

3.2. Adsorption of HU on the GP and its doped structures, $C_{30}B_9N_9$, $C_{16}B_{16}N_{16}$, $C_6B_{21}N_{21}$, and $B_{24}N_{24}$ nanosheets

The HU drug was adsorbed at the middle of the nanosheets in a parallel configuration to investigate the adsorption phenomenon of HU on the pristine GP and doped GP. Previous studies suggested that drug molecules were effectively adsorbed on the nanosheets when placed in a parallel way.[67] As a result, we have placed HU in a parallel way on the nanosheets and all complexes were then optimized. After optimization, we found

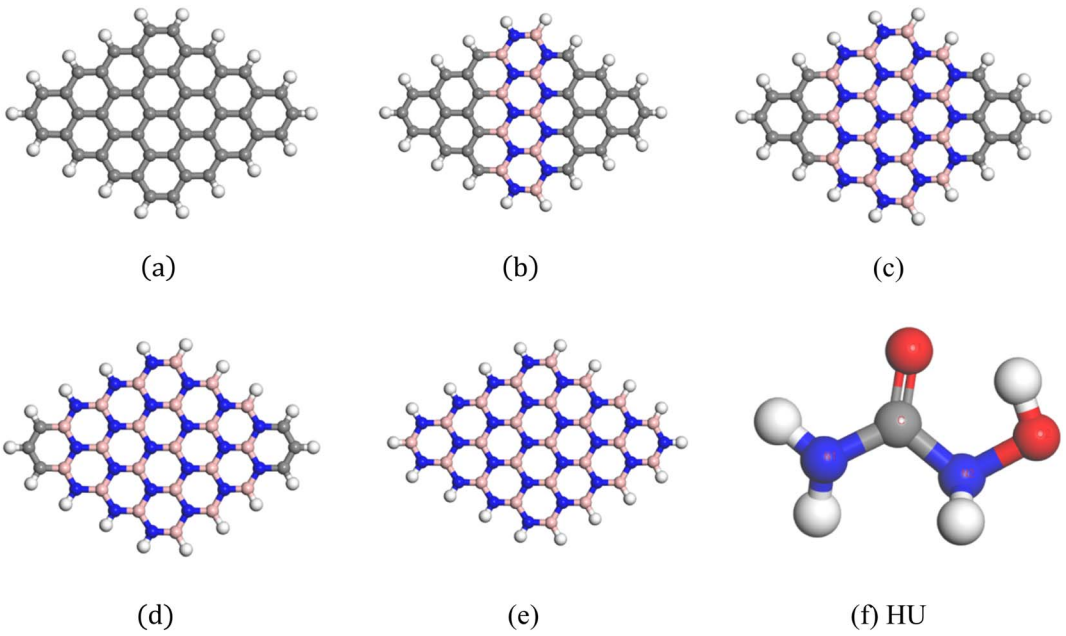

Fig. 1 Optimized geometric structures: (a) C_{48}, (b) $C_{30}B_9N_9$, (c) $C_{16}B_{16}N_{16}$, (d) $C_6B_{21}N_{21}$, (e) $B_{24}N_{24}$, and (f) HU.

that all complexes showed stability because no high structural deformation occurred, as shown in Fig. 2. The adsorption energies were found to be 0.14, −0.70, −3.03, −2.47 and −1.96 eV for the structures of HU/C_{48}, HU/$C_{30}B_9N_9$, HU/$C_{16}B_{16}N_{16}$, HU/$C_6B_{21}N_{21}$ and HU/$B_{24}N_{24}$, respectively, and the data are tabulated in Table 1. The adsorption energies with a positive value indicate an endothermic reaction, and a negative value indicates an exothermic reaction. In our adsorption energy calculations, the negative value of the adsorption energies was found for all complexes (except HU/C_{48}), which assures the probability of HU drug adsorption in doped GP nanosheets, and indicates that the adsorption process is exothermic and geometrically stable.[68] The adsorption energy is greater than 1 eV for the complexes of HU/$C_{16}B_{16}N_{16}$, HU/$C_6B_{21}N_{21}$ and HU/$B_{24}N_{24}$. As a result, these complexes are more stable and there is a low chemisorption occurrence. The HU drug prefers to adsorb on the $C_{30}B_9N_9$, $C_{16}B_{16}N_{16}$, $C_6B_{21}N_{21}$ and $B_{24}N_{24}$ nanosheets at a distance of about 7.45, 3.99, 7.20 and 7.21 Å, respectively. During the interaction with HU, Mulliken charge analysis was considered and calculated by the following equation,

$$\text{Charge transfer, } Q = Q_a - Q_b \quad (8)$$

where, Q_a and Q_b are the net charge after and before adsorption of HU on the nanosheets, respectively. Before adsorption on the nanosheets, the net charge transfer on the drug molecule is zero. However, after adsorption on the nanosheets, it loses or gains some amount of charge.[69] The positive and negative values of net charges on the drug indicate the losses and gains of charge from the nanosheets, respectively. According to the Mulliken charge analysis, during the interaction of HU on these four nanosheets, a small amount of charge of about 0.072*e*, 0.01*e*, 0.012*e*, and 0.014*e* was transferred from HU to the proposed nanosheets, respectively. So, the HU drug molecule performs like an electron donor, and GP and doped GP perform like an electron acceptor. Therefore, low negative values of adsorption energies with high interaction distance and a small amount of charge transfer imply that C_{48}, $C_{30}B_9N_9$, and $C_6B_{21}N_{21}$ are less sensitive towards the HU drug. Frontier molecular orbital (FMO) and energy gap (E_g) analyses were performed, and the results are tabulated in Table 2. Fig. 3 shows the FMO maps of the stable complexes of the HU/nanosheets. The HOMO levels were located at −4.02, −3.87, −3.76, and −5.83 eV for $C_{30}B_9N_9$, $C_{16}B_{16}N_{16}$, $C_6B_{21}N_{21}$ and $B_{24}N_{24}$ nanosheets, respectively. After adsorption of HU on the nanosheets, the HOMO and LUMO levels varied. For example, for the $C_{16}B_{16}N_{16}$ structure, the HOMO levels were reduced from −3.87 to −3.85 eV, while the LUMO levels increased from −3.69 to −3.71 eV. The HOMO and LUMO gap, *i.e.*, the energy gap, was also calculated. It was found that the energy gap was reduced from 0.17 to 0.15 eV for the $C_{16}B_{16}N_{16}$ nanosheets. The

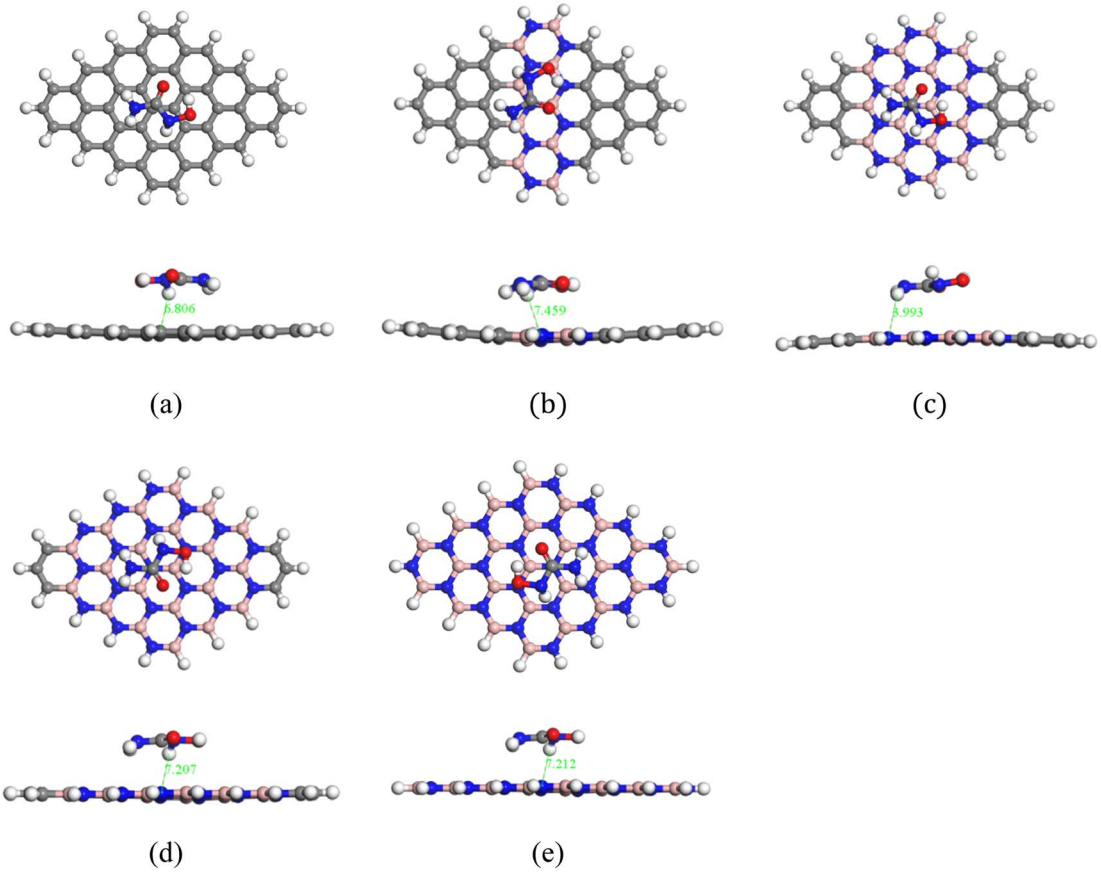

Fig. 2 Top and side views of the optimized complexes: (a) HU/C_{48}, (b) HU/$C_{30}B_9N_9$, (c) HU/$C_{16}B_{16}N_{16}$, (d) HU/$C_6B_{21}N_{21}$, and (e) HU/$B_{24}N_{24}$.

Table 1 Calculated adsorption energy (E_{ad}) in (eV), charge transfer (Q) in (e), and minimum interaction distance (d) in (Å)

	Air media			Water media		
Structures	E_{ad} (eV)	Q (e)	d (Å)	E_{ad} (eV)	Q (e)	d (Å)
HU/$C_{30}B_9N_9$	−0.70	0.072	7.45	−0.34	0.022	3.82
HU/$C_{16}B_{16}N_{16}$	−3.03	0.01	3.99	−0.288	0.015	3.84
HU/$C_6B_{21}N_{21}$	−2.47	0.012	7.20	−0.148	0.017	4.21
HU/$B_{24}N_{24}$	−1.96	0.014	7.21	−0.260	0.009	3.91

electronic properties, such as HOMO energy, LUMO energy and energy gap, were also calculated in water media. The HOMO level is located at −4.02 eV for the structure of $C_{16}B_{16}N_{16}$, but the LUMO level is located at the value of −3.91 eV before adsorption. After the adsorption of the drug towards the $C_{16}B_{16}N_{16}$ nanosheet, the HOMO and LUMO levels were located at 4.02 and −3.92 eV, respectively. Compared with the gas phase, the adsorption behaviour of HU on the $C_{16}B_{16}N_{16}$ nanosheet is slightly reduced in water media. Our observation is consistent with a previous study by Larijani H. Tavassoli *et al.*, where they found that the adsorption energy between the glycine and h-BN nanosheet was reduced from 0.325 to 0.233 eV in water solvent media.[70] A molecule with lower E_g is more polarizable, and normally shows low kinetic stability and high chemical reactivity.[71] As a result, the $C_{16}B_{16}N_{16}$ nanosheet shows high chemical reactivity towards the HU drug. Density of states (DOS) analysis provides a better understanding of the distribution of electronic states in a carrier complex as a function of energy. Fig. 4 shows the DOS and PDOS spectra of the pristine and doped nanosheets. When drug molecules interact with the carrier, they introduce additional electronic states within the system. These new states usually overlap with existing states in the carrier complex, thus changing the energy landscape. The introduction of drug molecules can increase the density of electronic states near the Fermi level, which is the energy level where electrons are generally found. This increase in density near the Fermi level indicates a reduction in the energy gap between occupied and unoccupied states within the system. PDOS analysis gives a more detailed examination of the contributions of individual atoms or orbitals to the electronic structure of the complex. Researchers can identify the specific atomic orbitals involved in interactions with drug molecules by studying the PDOS spectra. Upon interaction with drug molecules, the energy levels of atomic orbitals within the carrier complex may undergo shifts. Changes in the local environment around the atoms involved in binding the drug molecules can cause these shifts. This can result in the energy levels of relevant orbitals moving closer to the Fermi level, causing a reduction in the energy gap between the occupied and unoccupied states. The interaction between drug molecules and carrier complexes can also lead to changes in the hybridization of atomic orbitals, resulting in the formation of new electronic states within the energy gap. These hybridized states contribute to the overall reduction in the energy gap observed in the DOS spectra. As a result, DOS and PDOS spectra provide valuable insights into the electronic structure of carrier complexes in drug delivery systems, and the impact of drug molecule interactions on their energy landscape. The reduction in the energy gap between electronic states, as shown by these spectra, reflects the complex interplay between the carrier materials and drug molecules, ultimately influencing the efficiency and kinetics of drug delivery processes. The conductivity (σ) of this nanosheets was exponentially enhanced due to the reduction in the energy gap (E_g), and maintained the following relation:[72]

$$\sigma \propto e^{-\frac{E_g}{2KT}} \quad (9)$$

where, K is Boltzmann's constant $= 1.380 \times 10^{-23}$ m^2 kg^{-2} K^{-1}.

The electronic configuration of an atom, which is defined by the distribution of electrons in atomic orbitals, influences its chemical properties and behavior. Through an analysis of the electron density (ED) and electrostatic potential (ESP), we can predict the reactivity of molecules and identify reactive sites. Fig. 5 and 6 display the ED and ESP maps of the complexes, respectively. From the ED maps of the complexes, it is evident that there is an overlap of the electron density of HU and the nanosheets, indicating their interaction. The ESP maps of the complexes show that the color pink represents a high electron density region, indicating that electrons can be donated to other species. Therefore, this region is considered a negative reactive zone. Conversely, the color violet, which covers the drug molecule, represents the positive reactive zone because it can accept electrons from other species.

3.3. Dipole moment

The dipole moment is a crucial factor in studying the interaction between an absorbent and a drug. It can also help to explain the asymmetric charge distribution and reactivity of a system. A molecule is considered non-polar when the value of its dipole moment is zero.[73] The dipole moments of the different nanosheets and complexes are tabulated in Table 2. A

Table 2 HOMO energy (E_{HOMO}), LUMO energy (E_{LUMO}), HOMO–LUMO energy gap (E_g) in (eV), and dipole moment (D.M.) in Debye of the complexes

	Air media				Water media			
Structures	E_{HOMO}	E_{LUMO}	E_g	D.M.	E_{HOMO}	E_{LUMO}	E_g	D.M.
HU/$C_{30}B_9N_9$	−4.05	−3.76	0.287	3.11	−4.22	−3.94	0.28	11.23
HU/$C_{16}B_{16}N_{16}$	−3.85	−3.71	0.15	3.29	−4.02	−3.91	0.109	16.36
HU/$C_6B_{21}N_{21}$	−3.87	−3.69	0.18	5.13	−4.02	−3.68	0.333	18.75
HU/$B_{24}N_{24}$	−5.25	−1.46	3.79	8.66	−5.82	−1.71	4.10	12.77

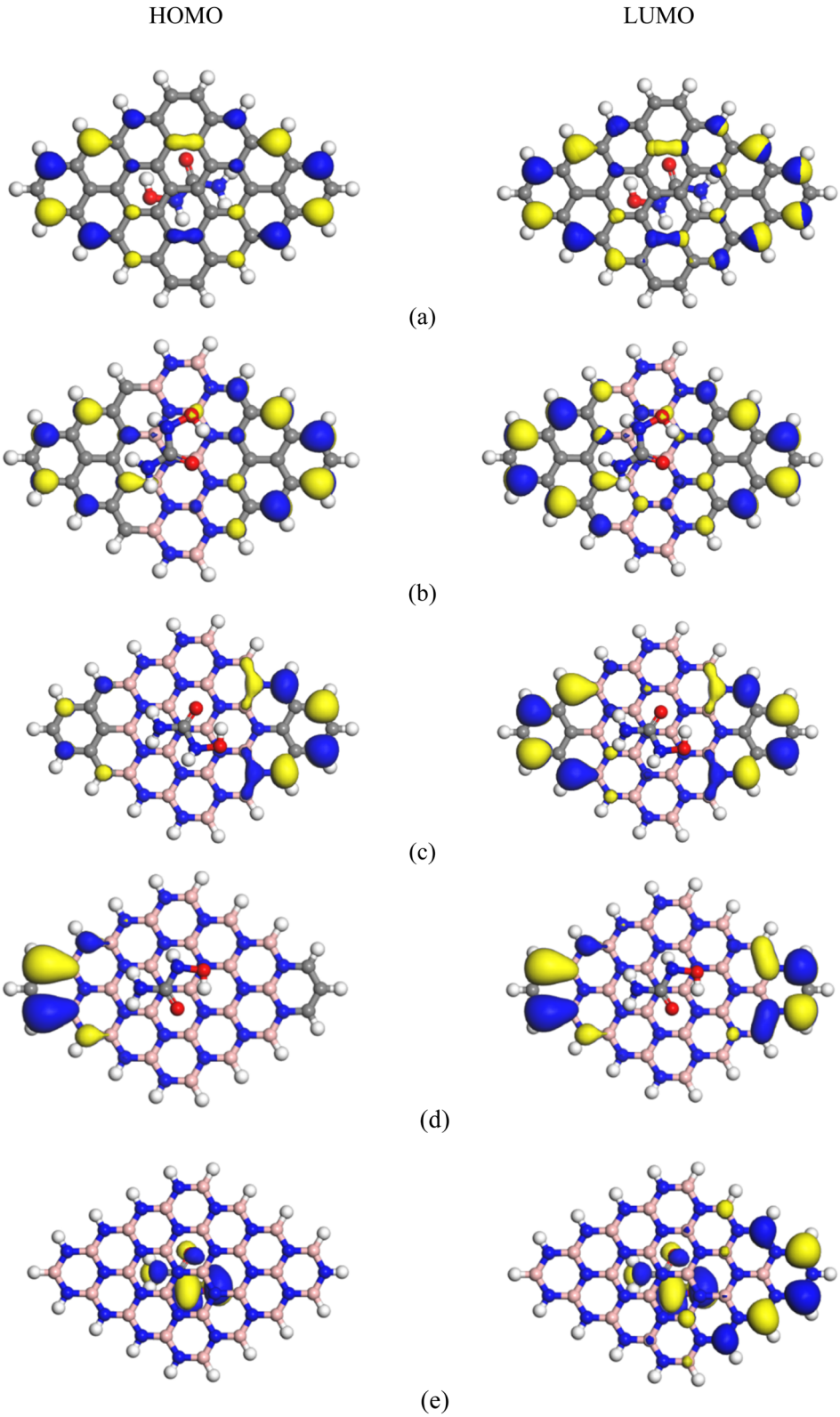

Fig. 3 HOMO and LUMO maps of the complexes: (a) HU/C_{48}, (b) HU/$C_{30}B_9N_9$, (c) HU/$C_{16}B_{16}N_{16}$, (d) HU/$C_6B_{21}N_{21}$, and (e) HU/$B_{24}N_{24}$.

high dipole moment value indicates more reactivity and solubility in polar solvents. After the adsorption of the HU drug on the nanosheets, the dipole moment increased, indicating that the HU drug can move easily in biochemical systems. The dipole moments of C_{48}, $C_{30}B_9N_9$, $C_{16}B_{16}N_{16}$, $C_6B_{21}N_{21}$ and $B_{24}N_{24}$ nanosheets were 0.0001, 3.17, 3.79, 4.48 and 6.54 D before the

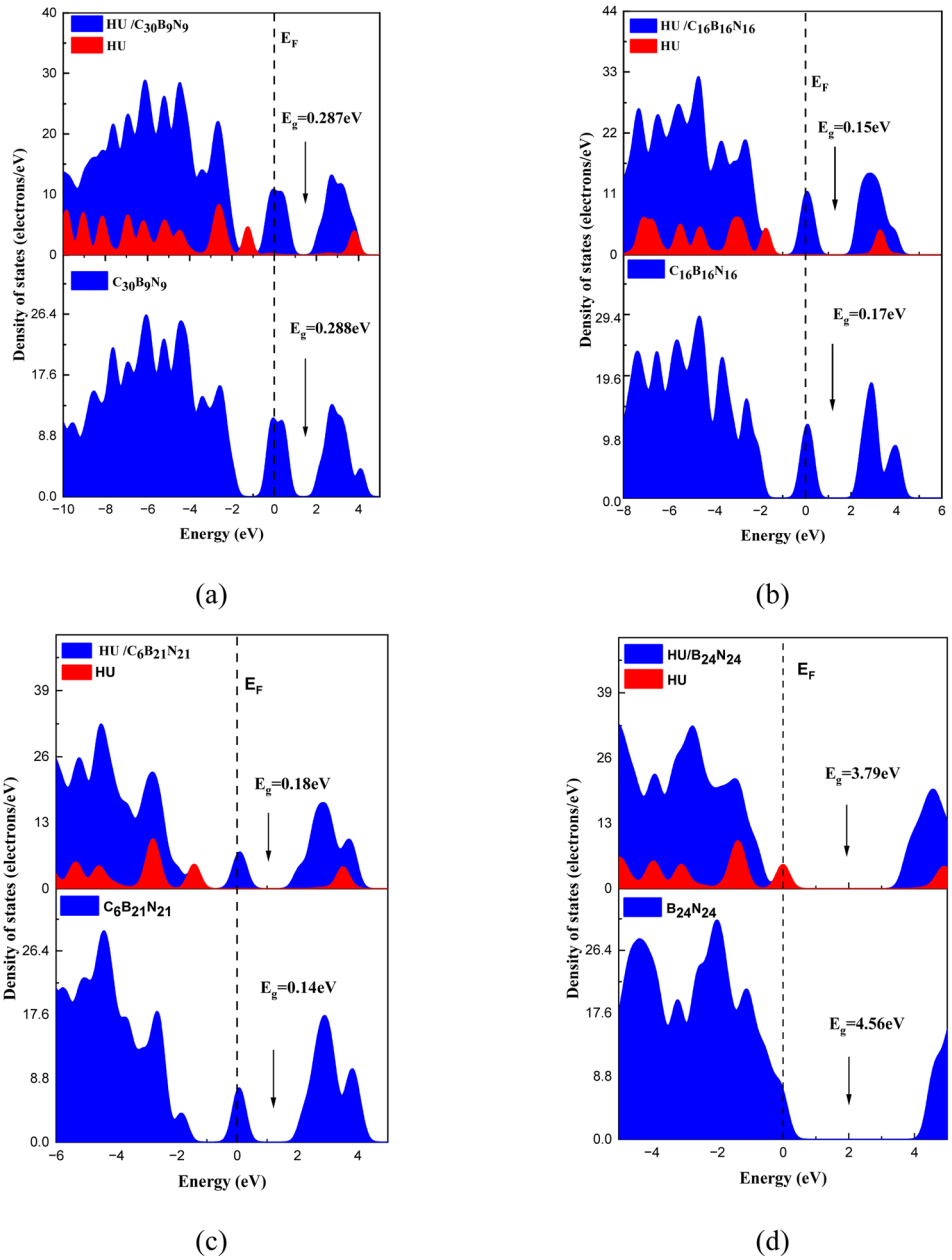

Fig. 4 DOS and PDOS spectra of the pristine, doped nanosheets, and their complexes: (a) $C_{30}B_9N_9$, (b) $C_{16}B_{16}N_{16}$, (c) $C_6B_{21}N_{21}$, and (d) $B_{24}N_{24}$.

adsorption process, respectively. After HU interacted with the nanosheets, the dipole moments rose and these values changed to 1.95, 5.13 and 8.66 D for the C_{48}, $C_6B_{21}N_{21}$ and $B_{24}N_{24}$ nanosheets, respectively, except for $C_{30}B_9N_9$ and $C_{16}B_{16}N_{16}$ nanosheets. The dipole moment of the $C_{16}B_{16}N_{16}$ nanosheet was found to be higher compared to that of the C_{48} and $C_{30}B_9N_9$ nanosheets. The increased dipole moments of the nanosheets have made them more soluble in polar media. The charge-transfer analysis and dipole moment analysis indicate that C_{48}, $C_6B_{21}N_{21}$, and $B_{24}N_{24}$ have the highest reactivity among these complexes. Interestingly, these two complexes (C_{48}, $B_{24}N_{24}$) have also shown increased reactivity in water solvent media due to their high dipole moment in the media. The dipole moment of the two nanosheets was enhanced by about 2 or 3 times after adsorption of the HU drug. The dipole moments of nanosheets in water solvent media were 0, 14.48, 19.84, 22.04, and 8.04 D. However, after interaction with the HU drug, the dipole moments increased to 5.20 and 12.77 D for the structures of C_{48} and $B_{24}N_{24}$, respectively. A bar diagram comparing the dipole moments is shown in Fig. 7 in air and water media.

3.4. Quantum molecular descriptors

Quantum molecular descriptors, such as the chemical potential (μ), global hardness (η), global softness (s), and electrophilicity index (ω) have been investigated to predict the reactivity of the

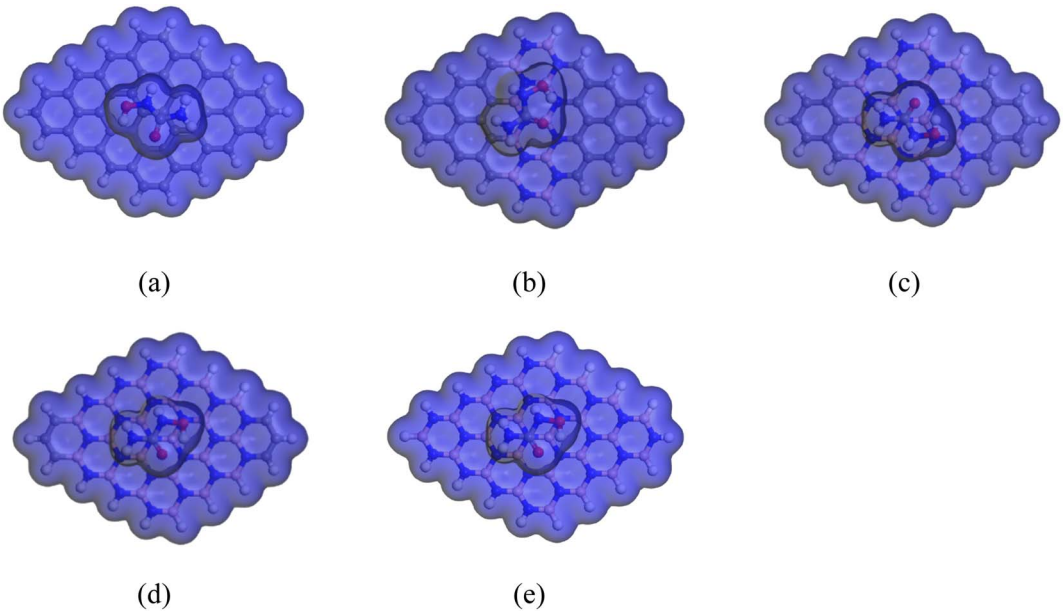

Fig. 5 ED maps of the complexes: (a) HU/C_{48}, (b) HU/$C_{30}B_9N_9$, (c) HU/$C_{16}B_{16}N_{16}$, (d) HU/$C_6B_{21}N_{21}$, and (e) HU/$B_{24}N_{24}$.

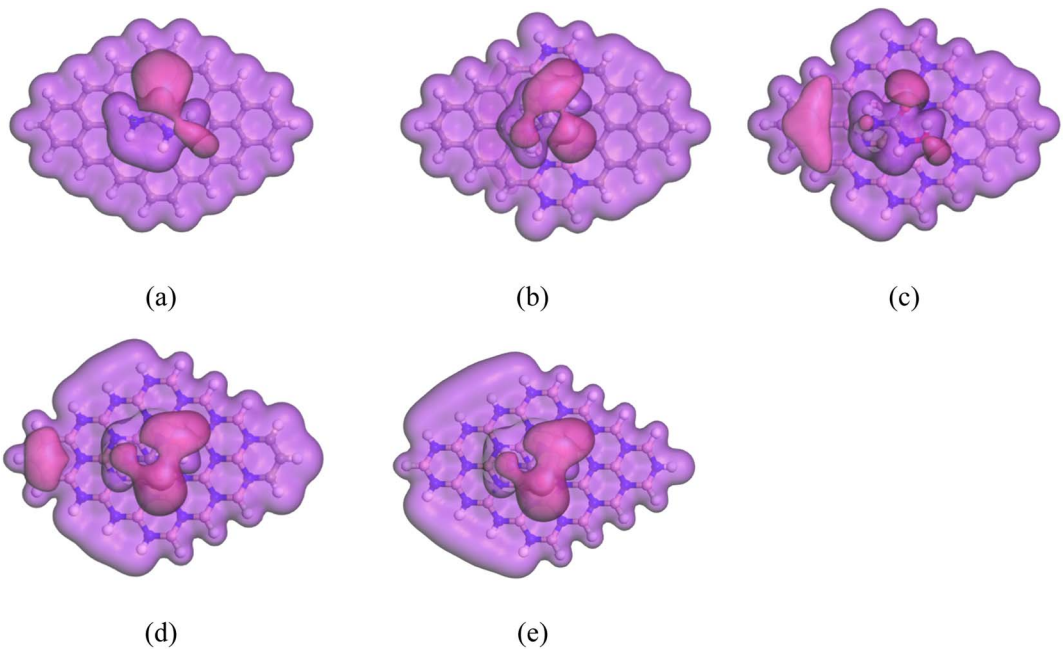

Fig. 6 ESP maps of the complexes: (a) HU/C_{48}, (b) HU/$C_{30}B_9N_9$, (c) HU/$C_{16}B_{16}N_{16}$, (d) HU/$C_6B_{21}N_{21}$, and (e) HU/$B_{24}N_{24}$.

nanosheets toward the HU drug.[74] The descriptors used in this study were based on the ionization potential and electron affinity, which, in practice, are just the negative energy of the highest occupied molecular orbital and lowest unoccupied molecular orbital. The calculated values for these descriptors are presented in Table 3. The electronic chemical potential (μ) value describes the escaping tendency of an electron from its equilibrium position.[75,76] The large chemical potential values are associated with high chemical reactivity.[77] The results of the study showed that the chemical potentials of the nanosheets increased after the adsorption of the HU drug. The calculated chemical potentials for C_{48}, $C_{30}B_9N_9$, $C_{16}B_{16}N_{16}$, $C_6B_{21}N_{21}$ and $B_{24}N_{24}$ nanosheets were 3.98, 3.88, 3.78, 3.69, and 3.55 eV, respectively. After adsorption of HU on the nanosheets, the values were enhanced to 3.99, 3.91, 3.78, and 3.78 eV, respectively, except $B_{24}N_{24}$.

The global hardness and softness are two important parameters that define the reactivity of complexes. When an external electric field is present, the resistance to deform a structure indicates the global hardness value.[78] The

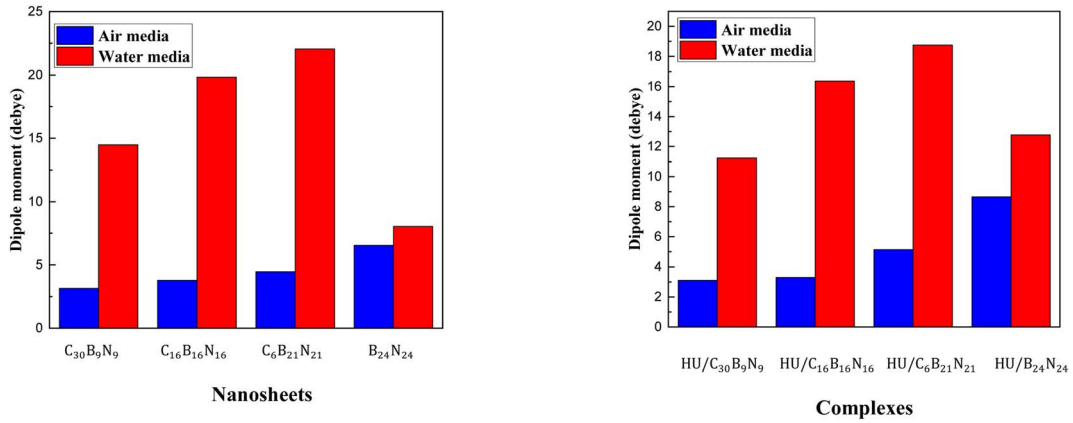

Fig. 7 Comparison of the dipole moment between the cases in the air and in water media before and after adsorption.

enhancement of the global hardness specifies the greater chemical stability of a structure, which indicates the decrease of the chemical reactivity.[79] Conversely, global softness has an inverse relation with global hardness. Higher global softness values indicate a higher reactivity of the nanosheets with the HU drug. In our observation, all nanosheets, except C_{48} and $C_6B_{21}N_{21}$, exhibited reactivity after adsorption of the HU drug, as confirmed by the decreasing values of the global hardness and increasing values of the global softness in the gas phase and water solvent media, as shown in Table 3. For example, the global hardness and softness values for the structure of $C_{16}B_{16}N_{16}$ were 0.087 eV and 5.75 eV^{-1}, respectively, before adsorption. After adsorption with the HU drug, the global hardness value decreases, and the global softness value increases, and these values are 0.074 eV and 6.71 eV^{-1}, respectively, indicating a high reactivity with the HU drug. Thus, the global hardness and softness analysis predicts that the chemical stability of the complexes is decreased, but the chemical reactivity is increased. The electrophilicity index (ω) was also calculated to investigate the electrophilic power, *i.e.*, the ability of the nanosheets to accept electrons.[80] The calculated values of ω are found to be 25.10, 52.20, 82.20, 97.50 and 2.80 eV for C_{48}, $C_{30}B_9N_9$, $C_{16}B_{16}N_{16}$, $C_6B_{21}N_{21}$ and $B_{24}N_{24}$ nanosheets, respectively. However, after adsorption of the HU drug on the nanosheets, the values of ω are increased to 25.31, 53.30, 95.90 and 2.97 eV, respectively, except for the $C_6B_{21}N_{21}$/HU complex. Therefore, the enhancement of the global softness and global electrophilicity index and the detraction of the global hardness indicate that HU/$C_{16}B_{16}N_{16}$ are the most favorable complexes compared with the other complexes in both gas phase and water media, and may be used as a potential carrier to deliver the HU drug into the target site.

Table 4 Solvation energy of the nanosheets and complexes

Structures	Solvation energy (eV)
C_{48}	−0.52
$C_{30}B_9N_9$	−0.95
$C_{16}B_{16}N_{16}$	−3.21
$C_6B_{21}N_{21}$	−2.72
$B_{24}N_{24}$	−2.20
HU/C_{48}	−1.44
HU/$C_{30}B_9N_9$	−0.89
HU/$C_{16}B_{16}N_{16}$	−1.00
HU/$C_6B_{21}N_{21}$	−0.95
HU/$B_{24}N_{24}$	−1.06

Table 3 Values of the chemical potential (μ), global hardness (η), electrophilicity index (ω) in unit eV, nucleophilicity index, υ and global softness (s) in unit eV^{-1} in gaseous and solvent media

	Gas media					Water media				
Structures	μ	η	s	ω	υ	μ	η	s	ω	υ
C_{48}	3.98	0.315	1.58	25.10	0.039	4.20	0.317	1.57	27.78	0.035
$C_{30}B_9N_9$	3.87	0.144	3.47	52.20	0.019	4.08	0.138	3.61	60.25	0.016
$C_{16}B_{16}N_{16}$	3.78	0.087	5.75	82.20	0.012	3.96	0.055	9.0	141.88	0.007
$C_6B_{21}N_{21}$	3.69	0.07	7.14	97.50	0.010	3.85	0.163	3.05	45.50	0.021
$B_{24}N_{24}$	3.55	2.28	0.22	2.80	0.360	3.78	2.08	0.24	3.45	0.290
HU/C_{48}	3.99	0.314	1.59	25.31	0.039	4.16	0.316	1.58	27.42	0.036
HU/$C_{30}B_9N_9$	3.91	0.143	3.48	53.30	0.018	4.08	0.140	3.57	59.59	0.016
HU/$C_{16}B_{16}N_{16}$	3.78	0.074	6.71	95.90	0.010	3.96	0.054	9.17	144.34	0.006
HU/$C_6B_{21}N_{21}$	3.78	0.09	5.55	79.42	0.012	3.85	0.166	3.0	44.62	0.022
HU/$B_{24}N_{24}$	3.36	1.89	0.263	2.97	0.336	3.76	2.05	0.243	3.46	0.289

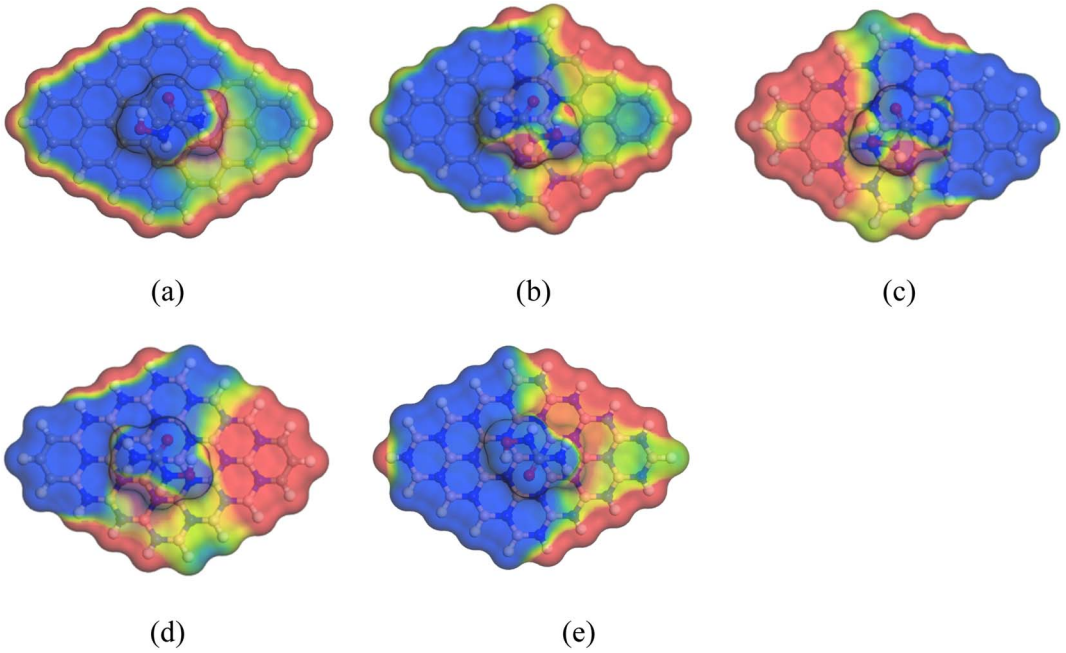

Fig. 8 Front views of the COSMO surfaces of the complexes: (a) HU/C_{48}, (b) HU/$C_{30}B_9N_9$, (c) HU/$C_{16}B_{16}N_{16}$, (d) HU/$C_6B_{21}N_{21}$, and (e) HU/$B_{24}N_{24}$.

3.5. Solvent effect

To determine the effect of solvent on the complexes, we calculated the solvation energy, adsorption energy, electronic properties, and dipole moment of the complexes in water media. The results are presented in Tables 1, 2 and 4. The solvation energy was calculated by the difference between the total energy of the complex in the water and air media, as shown below,

$$E_{solv} = E_{water} - E_{air} \quad (10)$$

The negative values of the solvation energy of the complexes indicated their stability and solubility in the solvent media. In our solvation energy calculations, all nanosheets showed good stability in water media due to their negative solvation energy. After adsorption of the HU on the nanosheets, the solvation energies became more negative, which implied their high stability in the water media. The calculated solvation energy values were −0.52, −0.95, −3.21, −2.72, and −2.20 eV for C_{48}, $C_{30}B_9N_9$, $C_{16}B_{16}N_{16}$, $C_6B_{21}N_{21}$ and $B_{24}N_{24}$ nanosheets, respectively. After interacting with the proposed nanosheets, the solvation energies for the complexes of HU/$C_{16}B_{16}N_{16}$ and HU/$B_{24}N_{24}$ were enhanced to −1.00 and −1.06 eV, respectively, compared to the complexes of HU/$C_{30}B_9N_9$ and HU/$C_6B_{21}N_{21}$. To further understand the solvent effect, we performed COSMO surface analysis of the complexes. The COSMO surfaces visualized the polar and non-polar regions of the complexes.

The red portion of the COSMO surface (shown in Fig. 8) represents the hydrogen bond donor (HBD) region, which is the positively charged region of the complexes. The blue portion represents the hydrogen bond acceptor (HBA) region, which is the negatively charged region of the complexes. The yellowish-green portion represents the neutral and non-polar regions of the complexes. Our analysis showed that after adding HU to the nanosheets, especially on the $C_{16}B_{16}N_{16}$ and $C_6B_{21}N_{21}$ nanosheets, the HBD region appeared large, implying the high polarity of the complexes in the water solvent media.

4. Conclusions

Nanomaterials have been studied extensively in recent years to reduce chemotherapy's direct side effects in cancer treatment. The aim is to find a suitable drug carrier that can quickly adsorb and desorb the drug in cancerous cells. The surface adsorption of HU on pristine graphene, doped graphene with alternative B and N and $B_{24}N_{24}$ nanosheets was investigated in gas and water media using DFT method. The adsorption energies, adsorption distances, charge transfer analysis, electronic properties (HOMO, LUMO and E_g), solvation energy, QMD and COSMO surface have been analyzed to visualize the adsorption behavior of HU on the nanosheets. Our calculation showed that, in gas media, the HU adsorbed on these four nanosheets ($C_{30}B_9N_9$, $C_{16}B_{16}N_{16}$, $C_6B_{21}N_{21}$ and $B_{24}N_{24}$) with adsorption energies of −0.70, −3.03, −2.47, and −1.96 eV by transferring 0.072, 0.01, 0.012, and 0.014*e* charges to the nanosheets, respectively. In water solvent media, the adsorption energies of $C_{30}B_9N_9$, $C_{16}B_{16}N_{16}$, $C_6B_{21}N_{21}$ and $B_{24}N_{24}$ were −0.82, −0.29, −0.15, and −0.26 eV, respectively. Charge transfer analysis predicted that about 0.022, 0.015, 0.017, and 0.009*e* charges were transferred from HU to the proposed nanosheets. The energy gaps of the structures were found to be 0.28, 0.15, 0.18 and 3.79 eV, respectively. From the DOS spectra, noticeable peaks appeared in the Fermi level after the adsorption of HU on the nanosheets,

which indicates the reduction of the energy gap. The reduction of E_g of the nanosheet by the HU drug dramatically enhances the electrical conductivity, which can be converted to an electrical signal. QMD analysis also showed that the $C_{16}B_{16}N_{16}$ nanosheet exhibited reactivity after adsorption of the HU drug, as confirmed by the decreasing values of the global hardness and increasing values of the global softness, nucleophilicity index in the gaseous as well, as water solvent medium. Therefore, it can be concluded that the $C_{16}B_{16}N_{16}$ nanosheet would be an appropriate carrier for the HU drug.

Data availability

The data supporting this article have been included in the manuscript.

Conflicts of interest

There are no conflicts to declare.

Acknowledgements

We thankfully acknowledge the Research Cell of Mawlana Bhashani Science and Technology University funded by UGC of Bangladesh (Grant No. 3631108) under the Ministry of Science and Technology (MOST) and the Bangladesh Research and Education Network (BdREN) for their computational access.

References

1 F. Bray, M. Laversanne, H. Sung, J. Ferlay, R. L. Siegel, I. Soerjomataram, *et al.*, Global cancer statistics 2022: GLOBOCAN estimates of incidence and mortality worldwide for 36 cancers in 185 countries, *Ca-Cancer J. Clin.*, 2024, **74**(3), 229–263.
2 R. A. Weinberg, How cancer arises, *Sci. Am.*, 1996, **275**(3), 62–70.
3 J. Simpson and J. H. Scholefield, Treatment of colorectal cancer: surgery, chemotherapy and radiotherapy, *Surgery*, 2008, **26**(8), 329–333.
4 M. S. Aslam, S. Naveed, A. Ahmed, Z. Abbas, I. Gull and M. A. Athar, Side effects of chemotherapy in cancer patients and evaluation of patients opinion about starvation based differential chemotherapy, *J. Cancer Ther.*, 2014, **5**, 817–822.
5 M. S. Mian, M. S. Rahman, J. Islam, K. N. Sakib, M. M. Tasnim and S. Yeasmin, In Situ Environmental Gamma Radiation Monitoring at Ramna Thana, Dhaka, Bangladesh: In Situ Environmental Gamma Radiation Monitoring, *J. Sci. Res.*, 2019, **11**(3), 263–272.
6 I. K. Sumi, M. S. Rahman, K. N. Sakib, M. M. Tasnim and S. Yeasmin, Outdoor Environmental Radiation Monitoring and Estimation of Radiation Risk on Public in New Market Thana, Dhaka, Bangladesh, *J. Sci. Res.*, 2021, **13**(3), 879–890.
7 W. B. Pratt, *The Anticancer Drugs*, Oxford University Press, 1994.
8 K. Madaan, D. Kaushik and T. Verma, Hydroxyurea: a key player in cancer chemotherapy, *Expert Rev. Anticancer Ther.*, 2012, **12**(1), 19–29.
9 W. F. C. Dresler and R. Stein, Ueber den hydroxylharnstoff, *Justus Liebigs Ann. Chem.*, 1869, **150**(2), 242–252.
10 N. Saban and M. Bujak, Hydroxyurea and hydroxamic acid derivatives as antitumor drugs, *Cancer Chemother. Pharmacol.*, 2009, **64**, 213–221.
11 H. Derendorf, *Drug Actions: Basic Principles and Theraputic Aspects*, CRC Press, 1995.
12 A. N. Schechter and G. P. Rodgers, Sickle cell anemia—basic research reaches the clinic, *N. Engl. J. Med.*, 1995, **332**, 1372–1374.
13 W. Y. Gao, A. Cara, R. C. Gallo and F. Lori, Low levels of deoxynucleotides in peripheral blood lymphocytes: a strategy to inhibit human immunodeficiency virus type 1 replication, *Proc. Natl. Acad. Sci. U. S. A.*, 1993, **90**(19), 8925–8928.
14 S. Cortelazzo, G. Finazzi, M. Ruggeri, O. Vestri, M. Galli, F. Rodeghiero, *et al.*, Hydroxyurea for patients with essential thrombocythemia and a high risk of thrombosis, *N. Engl. J. Med.*, 1995, **332**(17), 1132–1137.
15 M. Rosten, Hydroxyurea: a new antimetabolite in the treatment of psoriasis, *Br. J. Dermatol.*, 1971, **85**(2), 177–181.
16 P. B. Donovan, M. E. Kaplan, J. D. Goldberg, I. Tatarsky, Y. Najean, E. B. Silberstein, *et al.*, Treatment of polycythemia vera with hydroxyurea, *Am. J. Hematol.*, 1984, **17**(4), 329–334.
17 A. Soltani, M. T. Baei, E. T. Lemeski, S. Kaveh and H. Balakheyli, A DFT study of 5-fluorouracil adsorption on the pure and doped BN nanotubes, *J. Phys. Chem. Solids*, 2015, **86**, 57–64.
18 H. Zhang, M. Chhowalla and Z. Liu, 2D nanomaterials: graphene and transition metal dichalcogenides, *Chem. Soc. Rev.*, 2018, **47**(9), 3015–3017.
19 S. Das, S. U. D. Shamim, M. K. Hossain, F. Ahmed, M. A. Hossain and M. O. Rahman, A novel silicon-doped 2D Ti2C MXene monolayer as high capacity stable anode material for lithium ion batteries: insight from density functional theory study, *Appl. Surf. Sci.*, 2022, **600**, 154173.
20 A. Vaidyanathan, M. Mathew, S. Radhakrishnan, C. S. Rout and B. Chakraborty, Theoretical insight on the biosensing applications of 2D materials, *J. Phys. Chem. B*, 2020, **124**(49), 11098–11122.
21 H. L. Guo, X. F. Wang, Q. Y. Qian, F. B. Wang and X. H. Xia, A green approach to the synthesis of graphene nanosheets, *ACS Nano*, 2009, **3**(9), 2653–2659.
22 Z. Yang, R. Gao, N. Hu, J. Chai, Y. Cheng, L. Zhang, *et al.*, The prospective two-dimensional graphene nanosheets: preparation, functionalization and applications, *Nano-Micro Lett.*, 2012, **4**, 1–9.
23 S. Alwarappan, A. Erdem, C. Liu and C. Z. Li, Probing the electrochemical properties of graphene nanosheets for biosensing applications, *J. Phys. Chem. C*, 2009, **113**(20), 8853–8857.
24 S. Sattari, M. Adeli, S. Beyranvand and M. Nemati, Functionalized graphene platforms for anticancer drug delivery, *Int. J. Nanomed.*, 2021, 5955–5980.

25 X. Li, Y. Wang, L. Shi, H. Ma, Y. Zhang, B. Du, *et al.*, A novel ECL biosensor for the detection of concanavalin A based on glucose functionalized NiCo2S4 nanoparticles-grown on carboxylic graphene as quenching probe, *Biosens. Bioelectron.*, 2017, **96**, 113–120.
26 F. Xiao, M. Wang, F. Wang and X. Xia, Graphene–ruthenium (II) complex composites for sensitive ECL immunosensors, *Small*, 2014, **10**(4), 706–716.
27 C. I. Wang, W. C. Wu, A. P. Periasamy and H. T. Chang, Sensitive and selective DNA probe based on "turn-on" photoluminescence of C-dots@ RGO, *Anal. Bioanal. Chem.*, 2014, **406**, 6917–6923.
28 J. Liu, L. Cui and D. Losic, Graphene and graphene oxide as new nanocarriers for drug delivery applications, *Acta Biomater.*, 2013, **9**(12), 9243–9257.
29 S. Bhandary and B. Sanyal, *Graphene-Boron Nitride Composite: A Material with Advanced Functionalities*, INTECH Open Access, 2012, pp. 1–14.
30 L. Ci, L. Song, C. Jin, D. Jariwala, D. Wu, Y. Li, *et al.*, Atomic layers of hybridized boron nitride and graphene domains, *Nat. Mater.*, 2010, **9**(5), 430–435.
31 K. N. Munny, T. Ahmed, A. A. Piya and S. U. D. Shamim, Exploring the adsorption performance of doped graphene quantum dots as anticancer drug carriers for cisplatin by DFT, PCM, and COSMO approaches, *Struct. Chem.*, 2023, **34**(6), 2089–2105.
32 Y. Duan, H. Fu, L. Zhang, R. Gao, Q. Sun, Z. Chen, *et al.*, Embedding of ultra-dispersed MoS2 nanosheets in N, O heteroatom-modified carbon nanofibers for improved adsorption of Hg2+, *Compos. Commun.*, 2022, **31**, 101106.
33 D. Arumugam, M. Subramani, R. Durai, A. Sambasivam and S. Ramasamy, Probing the influence of defects and Si-doping in graphene sheet as an efficacious carrier for drug delivery system in gas and aqua phases-combined DFT and classical MD simulation, *J. Phys. Chem. Solids*, 2023, **181**, 111562.
34 H. O. Edet, H. Louis, T. E. Gber, P. S. Idante, T. C. Egemonye, P. B. Ashishie, *et al.*, Heteroatoms (B, N, S) doped quantum dots as potential drug delivery system for isoniazid: insight from DFT, NCI, and QTAIM, *Heliyon*, 2023, **9**(1), 1–12.
35 D. Golberg, Y. Bando, Y. Huang, T. Terao, M. Mitome, C. Tang, *et al.*, Boron nitride nanotubes and nanosheets, *ACS Nano*, 2010, **4**(6), 2979–2993.
36 H. Zeng, C. Zhi, Z. Zhang, X. Wei, X. Wang, W. Guo, *et al.*, "White graphenes": boron nitride nanoribbons via boron nitride nanotube unwrapping, *Nano Lett.*, 2010, **10**(12), 5049–5055.
37 Q. Weng, X. Wang, X. Wang, Y. Bando and D. Golberg, Functionalized hexagonal boron nitride nanomaterials: emerging properties and applications, *Chem. Soc. Rev.*, 2016, **45**(14), 3989–4012.
38 M. H. Rocky, M. Khatun, A. Al Roman, D. Roy and M. T. Ahmed, A DFT study on boron carbon nitride and in-plane graphene-boron nitride nanosheets for O3 and F2 gas sensing, *Comput. Theor. Chem.*, 2024, **1237**, 114639.
39 M. T. Ahmed, D. Roy, A. Al Roman, Z. Kowser, S. Islam and F. Ahmed, The adsorption of CO gas on the surface of boron nitride incorporating 2D carbon allotropes: a DFT analysis, *Phys. Scr.*, 2024, **99**(6), 0659c7.
40 D. Roy, M. K. Hossain, S. M. Hasan, S. Khanom, M. A. Hossain and F. Ahmed, Half-metallic ferromagnetism induced by TM-TM atom pair co-doping in 2D hexagonal boron nitride monolayer: a first principle study, *Mater. Sci. Eng., B*, 2021, **271**, 115247.
41 F. Hui, C. Pan, Y. Shi, Y. Ji, E. Grustan-Gutierrez and M. Lanza, On the use of two dimensional hexagonal boron nitride as dielectric, *Microelectron. Eng.*, 2016, **163**, 119–133.
42 P. Marbaniang, I. Patil, M. Lokanathan, H. Parse, D. C. Sesu, S. Ingavale, *et al.*, Nanorice-like structure of carbon-doped hexagonal boron nitride as an efficient metal-free catalyst for oxygen electroreduction, *ACS Sustain. Chem. Eng.*, 2018, **6**(8), 11115–11122.
43 T. S. Ashton and A. L. Moore, Foam-like hierarchical hexagonal boron nitride as a non-traditional thermal conductivity enhancer for polymer-based composite materials, *Int. J. Heat Mass Tran.*, 2017, **115**, 273–281.
44 Y. Zhang, Z. Xia, Q. Li, G. Gui, G. Zhao, S. Luo, *et al.*, Copper/hexagonal boron nitride nanosheet composite as an electrochemical sensor for nitrite determination, *Int. J. Electrochem. Sci.*, 2018, **13**(6), 5995–6004.
45 P. Ahmad, M. U. Khandaker, N. Muhammad, F. Rehman, G. Khan, M. A. Rehman, *et al.*, Synthesis of multilayered hexagonal boron nitride microcrystals as a potential hydrogen storage element, *Ceram. Int.*, 2017, **43**(9), 7358–7361.
46 E. S. Permyakova, I. V. Sukhorukova, L. Y. Antipina, A. S. Konopatsky, A. M. Kovalskii, A. T. Matveev, *et al.*, Synthesis and characterization of folate conjugated boron nitride nanocarriers for targeted drug delivery, *J. Phys. Chem. C*, 2017, **121**(50), 28096–28105.
47 Q. Weng, B. Wang, X. Wang, N. Hanagata, X. Li, D. Liu, *et al.*, Highly water-soluble, porous, and biocompatible boron nitrides for anticancer drug delivery, *ACS Nano*, 2014, **8**(6), 6123–6130.
48 M. Jedrzejczak-Silicka, M. Trukawka, M. Dudziak, K. Piotrowska and E. Mijowska, Hexagonal boron nitride functionalized with Au nanoparticles—properties and potential biological applications, *Nanomaterials*, 2018, **8**(8), 605.
49 B. Delley, An all-electron numerical method for solving the local density functional for polyatomic molecules, *J. Chem. Phys.*, 1990, **92**(1), 508–517.
50 B. Delley, From molecules to solids with the DMol 3 approach, *J. Chem. Phys.*, 2000, **113**(18), 7756–7764.
51 J. P. Perdew, K. Burke and M. Ernzerhof, Generalized gradient approximation made simple, *Phys. Rev. Lett.*, 1996, **77**(18), 3865.
52 J. P. Perdew and A. Zunger, Self-interaction correction to density-functional approximations for many-electron systems, *Phys. Rev. B: Condens. Matter Mater. Phys.*, 1981, **23**(10), 5048.
53 W. Kohn, A. D. Becke and R. G. Parr, Density functional theory of electronic structure, *J. Phys. Chem.*, 1996, **100**(31), 12974–12980.

54 S. Grimme, Semiempirical GGA-type density functional constructed with a long-range dispersion correction, *J. Comput. Chem.*, 2006, **27**(15), 1787–1799.
55 B. Delley, Hardness conserving semilocal pseudopotentials, *Phys. Rev. B: Condens. Matter Mater. Phys.*, 2002, **66**(15), 155125.
56 H. p. Zhang, X. g. Luo, H. t. Song, X. y. Lin, X. Lu and Y. Tang, DFT study of adsorption and dissociation behavior of H2S on Fe-doped graphene, *Appl. Surf. Sci.*, 2014, **317**, 511–516.
57 Y. Inada and H. Orita, Efficiency of numerical basis sets for predicting the binding energies of hydrogen bonded complexes: evidence of small basis set superposition error compared to Gaussian basis sets, *J. Comput. Chem.*, 2008, **29**(2), 225–232.
58 M. J. Ungerer, C. Van Sittert, D. J. Van Der Westhuizen and H. M. Krieg, Molecular modelling of tantalum pentahalides during hydrolysis and oxidation reactions, *Comput. Theor. Chem.*, 2016, **1090**, 112–119.
59 B. Delley, The conductor-like screening model for polymers and surfaces, *Mol. Simul.*, 2006, **32**(2), 117–123.
60 S. S. U. Daula, M. K. Hossain, S. M. Hasan, A. Hossain and F. Ahmed, Ab initio study of N-doped graphene oxide (NDGO) as a promising anode material for Li-ion rechargeable battery, *Mol. Simul.*, 2020, **46**(14), 1135–1145.
61 P. K. Chattaraj and R. G. Parr, Density functional theory of chemical hardness, *Chemical Hardness*, 2005, pp. 11–25.
62 J. Khandogin and D. M. York, Quantum descriptors for biological macromolecules from linear-scaling electronic structure methods, *Proteins: Struct., Funct., Bioinf.*, 2004, **56**(4), 724–737.
63 R. G. Pearson, Absolute electronegativity and hardness: applications to organic chemistry, *J. Org. Chem.*, 1989, **54**(6), 1423–1430.
64 A. S. Rad, S. S. Shabestari, S. A. Jafari, M. R. Zardoost and A. Mirabi, N-doped graphene as a nanostructure adsorbent for carbon monoxide: DFT calculations, *Mol. Phys.*, 2016, **114**(11), 1756–1762.
65 M. Shahabi and H. Raissi, Investigation of the solvent effect, molecular structure, electronic properties and adsorption mechanism of Tegafur anticancer drug on graphene nanosheet surface as drug delivery system by molecular dynamics simulation and density functional approach, *J. Inclusion Phenom. Macrocyclic Chem.*, 2017, **88**, 159–169.
66 T. Ahmed, M. A. Rahman, R. Islam, A. A. Piya and S. U. D. Shamim, Unravelling the adsorption performance of BN, AlN, GaN and InN 2D nanosheets towards the ciclopirox, 5-fluorouracil and nitrosourea for anticancer drug delivery motive: A DFT-D with QTAIM, PCM and COSMO investigations, *Comput. Theor. Chem.*, 2022, **1214**, 113797.
67 S. N. Ema, M. A. Khaleque, A. Ghosh, A. A. Piya, U. Habiba and S. U. D. Shamim, Surface adsorption of nitrosourea on pristine and doped (Al, Ga and In) boron nitride nanosheets as anticancer drug carriers: The DFT and COSMO insights, *RSC Adv.*, 2021, **11**(58), 36866–36883.
68 W. L. Jorgensen and E. M. Duffy, Prediction of drug solubility from structure, *Adv. Drug Deliv. Rev.*, 2002, **54**(3), 355–366.
69 B. Mondal, K. Basu, R. Jana, P. Mondal, B. Hansda, A. Datta, *et al.*, Copper Nanoclusters for Catalytic Carbon–Carbon and Carbon–Nitrogen Bond Formations, *ACS Appl. Nano Mater.*, 2022, **5**(6), 7932–7943.
70 H. T. Larijani, M. Jahanshahi, M. D. Ganji and M. H. Kiani, Computational studies on the interactions of glycine amino acid with graphene, h-BN and h-SiC monolayers, *Phys. Chem. Chem. Phys.*, 2017, **19**(3), 1896–1908.
71 K. Fukui, Role of frontier orbitals in chemical reactions, *Science*, 1982, **218**(4574), 747–754.
72 J. Mawwa, S. U. D. Shamim, S. Khanom, M. K. Hossain and F. Ahmed, In-plane graphene/boron nitride heterostructures and their potential application as toxic gas sensors, *RSC Adv.*, 2021, **11**(52), 32810–32823.
73 T. Ahmed, M. A. Rahman, R. Islam, A. A. Piya and S. U. D. Shamim, Unravelling the adsorption performance of BN, AlN, GaN and InN 2D nanosheets towards the ciclopirox, 5-fluorouracil and nitrosourea for anticancer drug delivery motive: a DFT-D with QTAIM, PCM and COSMO investigations, *Comput. Theor. Chem.*, 2022, **1214**, 113797.
74 R. Ziraoui, H. Meghraoui, M. El Gouri, M. Rafik and A. Elharfi, Synthesis and physico chemical study of a new hexa and tetra functional epoxy materials based on bis-para-terephthalylidene phosphoric ester, *J. Mater. Environ. Sci.*, 2010, **1**(4), 213–218.
75 U. Srimathi, V. Nagarajan and R. Chandiramouli, Interaction of Imuran, Pentasa and Hyoscyamine drugs and solvent effects on graphdiyne nanotube as a drug delivery system-a DFT study, *J. Mol. Liq.*, 2018, **265**, 199–207.
76 A. S. Rad and P. Valipour, Interaction of methanol with some aniline and pyrrole derivatives: DFT calculations, *Synth. Met.*, 2015, **209**, 502–511.
77 M. Vatanparast and Z. Shariatinia, Hexagonal boron nitride nanosheet as novel drug delivery system for anticancer drugs: insights from DFT calculations and molecular dynamics simulations, *J. Mol. Graph. Model.*, 2019, **89**, 50–59.
78 N. Islam and D. C. Ghosh, The electronegativity and the global hardness are periodic properties of atoms, *J. Quant. Inf. Sci.*, 2011, **1**(3), 135.
79 A. S. Rad, A. S. Alijantabar, N. Motaghedi, S. Maleki and M. Peyravi, Theoretical study of chemisorption of cyanuric fluoride and S-triazine on the surface of Al-doped graphene, *Mol. Simul.*, 2016, **42**(18), 1519–1527.
80 P. K. Chattaraj and D. R. Roy, Update 1 of: electrophilicity index, *Chem. Rev.*, 2007, **107**(9), PR46–PR74.